NIH Public Access
Author Manuscript
Vis Neurosci. Author manuscript; available in PMC 2014 February 27.

Published in final edited form as:
Vis Neurosci. 2013 July ; 30(4): 129–139. doi:10.1017/S0952523813000138.

Protein Partners of Dynamin-1 in the Retina

Gregory H. Grossman[1], **Lindsey A. Ebke**[1], **Craig D. Beight**[1], **Geeng-Fu Jang**[1], **John W. Crabb**[1,2], and **Stephanie A. Hagstrom**[1,2]

[1]Cole Eye Institute and Lerner Research Institute, Cleveland Clinic, Cleveland, OH

[2]Departments of Ophthalmology and Molecular Medicine, Cleveland Clinic Lerner College of Medicine of Case Western Reserve University, Cleveland, OH

Abstract

Dynamin proteins are involved in vesicle generation, providing mechanical force to excise newly formed vesicles from membranes of cellular compartments. In the brain, dynamin-1, -2 and -3 have been well-studied; however, their function in the retina remains elusive. A retina-specific splice-variant of dynamin-1 interacts with the photoreceptor-specific protein Tubby-like Protein 1 (Tulp1), which when mutated causes an early-onset form of autosomal recessive retinitis pigmentosa. Here we investigated the role of the dynamins in the retina, using immunohistochemistry to localize dynamin-1, -2 and -3 and immunoprecipitation followed by mass spectrometry to explore dynamin-1 interacting proteins in mouse retina. Dynamin-2 is primarily confined to the inner segment compartment of photoreceptors, suggesting a role in outer segment protein transport. Dynamin-3 is present in the terminals of photoreceptors and dendrites of second-order neurons, but is most pronounced in the inner plexiform layer where second-order neurons relay signals from photoreceptors. Dynamin-1 appears to be the dominant isoform in the retina and is present throughout the retina and in multiple compartments of the photoreceptor cell. This suggests that it may function in multiple cellular pathways. Surprisingly, dynamin-1 expression and localization did not appear to be disrupted in *tulp1−/−* mice. Immunoprecipitation experiments reveal that dynamin-1 associates primarily with proteins involved in cytoskeletal-based membrane dynamics. This finding is confirmed by western blot analysis. Results further implicate dynamin-1 in vesicular protein transport processes relevant to synaptic and post-Golgi pathways and indicate a possible role in photoreceptor stability.

Keywords

photoreceptor; Dynamin-1; Tulp1; proteomics; vesicle

Introduction

The classical dynamins belong to a superfamily of GTPases that includes dynamin-like proteins (Ferguson & De Camilli, 2012). Dynamins participate in diverse membrane dynamics and vesicle trafficking functions, contributing mechanical force to excise newly formed vesicles from membranes of cellular components (McNiven *et al.*, 2000). Three genes in mammals encode the dynamin proteins: *DNM1*, *DNM2* and *DNM3* (Cao *et al.*, 1998). Of these, dynamin-2 is the only member that is ubiquitously expressed. Dynamin-1 is neuron-specific, while dynamin-3 expression is tissue specific, reportedly found in brain, testis, lung and heart (Cao *et al.*, 1998). All three dynamin isoforms are present in neuronal

Corresponding Author: Stephanie A. Hagstrom, Ph.D., Ophthalmic Research - i31, Cole Eye Institute, Cleveland Clinic, 9500 Euclid Avenue, Cleveland, OH 44195, hagstrs@ccf.org, Phone: 216-445-4133, Fax: 216-445-3670.

NIH-PA Author Manuscript
NIH-PA Author Manuscript
NIH-PA Author Manuscript

NIH-PA Author Manuscript

NIH-PA Author Manuscript

NIH-PA Author Manuscript

tissue. Determining the physiological role of the dynamins is a significant challenge as there are overlapping functions of the isoforms (Ferguson *et al.*, 2007; Raimondi *et al.*, 2011) yet splice variants of each isoform may perform separate cellular tasks (Cao *et al.*, 1998; McNiven *et al.*, 2000).

Dynamin -1, -2, and -3 proteins have been identified in mouse photoreceptor cells of the retina (Liu *et al.*, 2007); however, the extent of their expression in the retina has not been fully investigated. Only two diseases are associated with mutations in dynamin genes and both have a visual defect. Mutations in *DNM2* underlie an autosomal dominant form of intermediate Charcot-Marie-Tooth disease, a peripheral neuropathy that can result in vision loss (Zuchner *et al.*, 2005) and autosomal dominant centronuclear myopathy, which can induce a paralysis of the extraocular muscles (Jeub *et al.*, 2008). Given the importance of dynamins in the central nervous system, it would not be surprising if additional defects in dynamin gene products affect retinal physiology and induce ocular phenotypes. The photoreceptor cells have an extremely high energy requirement due in part to tonic synaptic signaling and extensive vesicular protein transport (Linton *et al.*, 2010). To meet this high demand, photoreceptors have developed specialized mechanisms to handle the continuous cycling of vesicles. How the dynamins contribute to these specialized features remains to be determined.

We previously identified a splice-variant of dynamin-1, termed dynamin-1 (a,c), which colocalizes and interacts with the photoreceptor-specific Tubby-like protein 1 (Tulp1) (Xi *et al.*, 2007). Mutations in *TULP1* cause a form of autosomal recessive retinitis pigmentosa, a type of inherited retinal degeneration which leads to blindness (Hagstrom *et al.*, 1998). As an approach to better understanding dynamin function in photoreceptor cells, we report here the characterization of dynamin isoform expression and localization in the mouse retina and the identification of possible dynamin-1 interacting proteins.

Methods

Mice

Generation and maintenance of *tulp1*−/− mice on a C57BL/6 background has been described previously (Hagstrom *et al.*, 1999). Control C57BL/6 mice were obtained from The Jackson Laboratory. Mice were euthanized by CO_2 inhalation followed by cervical dislocation. All animal experiments were approved by the Institutional Animal Care and Use Committee of the Cleveland Clinic and were performed in compliance with the National Institutes of Health guidelines.

Immunohistochemistry

Eyes from P16 mice were prepared as previously described (Xi *et al.*, 2007; Grossman *et al.*, 2011). Briefly, after removal of the cornea and lens, the posterior poles were fixed in 4% paraformaldehyde in PBS for 3 h. The eye cups were then immersed through a graded series of sucrose solutions: 10% for 1 h, 20% for 1 h and 30% overnight. The posterior pole was embedded in OCT freezing medium, flash frozen on powderized dry ice and immediately transferred to −80°C. The tissue was sectioned at 10-μm thickness using a cryostat (Leica, Wetzlar, Germany) at −30°C. For each genotype (wt and *tulp1*−/−), a minimum number of four sections from five different mice were examined for each antibody. Retinal sections were blocked in 5% bovine serum albumin and 1% normal goat serum with 0.1% Triton X-100 for 1 h before incubation with primary antibodies overnight at 4°C. A panel of well-characterized antibodies was used for immunostaining. Table 1 contains a complete list of antibodies, immunogens, sources, host species and dilutions used. After washing 3 times in PBS, sections were incubated in fluorescent secondary antibodies at room temperature for 1

NIH-PA Author Manuscript

NIH-PA Author Manuscript

NIH-PA Author Manuscript

h. Secondary antibodies were: Alexa Fluor ® 488 goat anti-rabbit IgG and goat anti-mouse IgG; Alexa Fluor® 594 goat anti-rabbit IgG and goat anti-mouse IgG (Invitrogen, Carlsbad, California, USA). The sections were then rinsed 3 times with PBS followed by a dH_2O rinse and coverslipped with Vectashield® mounting media with DAPI (Vector Laboratories, Burlingame, California, USA). Sections were imaged using an Olympus BX-61 fluorescent microscope (Olympus, Tokyo, Japan), equipped with a CCD monochrome camera (Hamamatsu Photonics, Bridgewater, New Jersey, USA).

Western Blot

Western blot analysis was performed as previously described with P16 mouse tissues from wt and *tulp1−/−* mice (n=2 for each genotype) (Hagstrom *et al.*, 2001; Xi *et al.*, 2005; Xi *et al.*, 2007). Briefly, proteins were separated on SDS-PAGE gels and electroblotted to PVDF membranes. Membranes were incubated with primary antibodies (Table 1), followed by peroxidase-conjugated secondary antibodies, and were detected by chemiluminescence.

Immunoprecipitation and Protein Identification

Immunoprecipitation (IP) with Dynabeads was performed according to the manufacturer (Dynabeads Protein A 100.06D, Invitrogen, Carlsbad, California, USA). IPs followed by protein identification by liquid chromatography tandem mass spectrometry (LC MS/MS) were performed using mouse retina and brain tissue. In separate experiments, IPs followed by Western blot analysis were performed using bovine retinal tissue or mouse brain and retinal tissue. Briefly, adult bovine retina (600 mg: ~1 retina), P16-P60 mouse retinas (300 mg: 30 retinas) or P16-P60 mouse brains (300 mg: ~ 1 brain) were homogenized in 3 mL of lysis buffer (50mM Tris pH 8.0, 150 mM NaCl, 10% glycerol, 0.5% Triton X-100, 0.1% NP40) supplemented with protease inhibitors (Roche Applied Science, Indianapolis, Indiana, USA). Homogenization was accomplished by freezing the tissue and manually grinding with a disposable pestle within a micro-centrifuge tube. This was repeated two additional cycles. The suspension was centrifuged 9,000 rpm for 15 min, and the supernatant containing the retinal lysates were transferred to a separate tube and the protein concentration (bovine: 4 μg/μl; mouse: 1.2 μg/μl) was determined by the BCA (bicinchoninic acid) assay (Thermo Scientific, Rockford, Illinois, USA). For IP, 10 μg of polyclonal anti-dynamin-1 antibody (Thermo Scientific, Rockford, Illinois, USA), or non-specific rabbit IgG (Southern Biotech, Birmingham, Alabama, USA) was used for each 500 μl of retinal lysate. Immediately prior to IP, the antibody was crosslinked to the beads using BS^3 (Bis[sulfosuccinimidyl] suberate) (Thermo Scientific, Rockford, Illinois, USA) for 30 min at room temperature. The IP binding reactions proceeded overnight at 4°C, followed by 3 washes with buffer. Proteins were then eluted with 20 μl of SDS sample buffer. Immunoprecipitated antigens were fractionated by SDS-PAGE on a 4–20% Tris-glycine 5-well gel (Invitrogen) with 60 μl of each IP product loaded per gel lane. The gel was then stained with colloidal Coomassie blue (Gel Code Blue, Pierce, Rockford, IL) and a disposable gridcutter (Gel Company Inc, San Francisco, California, USA) was used to excise 2 mm serial sections from each lane containing the IP products. Each gel sample was digested *in situ* with trypsin and proteins identified by LC MS/MS using a quadrupole time-of-flight (QTOF) instrument and Cap LC system (CapLC System; Waters Corporation, Milford, Massachusetts, USA), as described previously (Crabb *et al.*, 2002; Xi *et al.*, 2003; Xi *et al.*, 2005; Xi *et al.*, 2007). Protein identifications utilized ProteinLynx Global Server software (Waters Corporation), Mascot 2.2 (Matrix Science, Boston, Massachusetts, USA) and the Swiss-Protein murine sequence database (May 2012 release, 16529 total mouse sequences). Bioinformatic functional analyses were performed with Ingenuity Pathway Analysis (Summer Release, June 2012, Ingenuity Systems, Redwood City, California, USA, www.ingenuity.com), and the UniProtKB/Swiss-Prot protein database (web.expasy.org/docs/)

NIH-PA Author Manuscript

NIH-PA Author Manuscript

NIH-PA Author Manuscript

Results

All dynamin isoforms are expressed in the mouse retina

Western blot analysis shows that all three dynamin isoforms are expressed in the mouse retina (Fig. 1). All studies were conducted at P16, an age at which all of the cell types of the retina are present in wt mice, but which precedes photoreceptor cell death in *tulp1*−/− mice (Hagstrom *et al.*, 1999; Grossman *et al.*, 2009; Grossman *et al.*, 2011). Dynamin-1, the neuronal-specific isoform, was detected in the retina and brain at its known molecular weight of 100 kDa, but not in testis (Fig. 1A). This is in agreement with previous findings (Cao *et al.*, 1998; Ferguson *et al.*, 2007). In western blots probed with dynamin-2 antibodies, immunoreactive bands were present at ~100 kDa in all tissues examined (Fig. 1B), in agreement with studies supporting the ubiquitous expression of this isoform (Cao *et al.*, 1998; Ferguson *et al.*, 2007). We detected dynamin-3 as a component of the retina, as well as the brain and testis (Fig. 1C).

Because of the association between Tulp1 and dynamin-1 (a,c) in the retina (Xi *et al.*, 2007), we examined whether dynamin-1 expression is altered in the absence of Tulp1. Western blot analysis of wt and *tulp1*−/− retinal lysates probed with a dynamin-1 specific antibody identified one band at approximately 100 kDa in both lysates (Fig. 2A). Probing with antibodies against actin supported equal protein loading across lanes. Our results suggest that dynamin-1 protein expression levels are not severely altered in the absence of Tulp1. Western blots of wt and *tulp1*−/− retinal lysates probed with dynamin-2 (Fig. 2B) and dynamin-3 (Fig. 2C) antibodies also showed that their levels were not grossly affected by the absence of Tulp1.

Differential localization of dynamin isoforms in the mouse retina

The distribution of the dynamin isoforms in P16 mouse retinas was examined by immunohistochemistry (IHC) (Fig. 3). A minimum of four sections from five different mouse retinas were examined for each experiment. Figure 3A shows that dynamin-1 is localized to the inner segment (IS), cell bodies and axons of the outer nuclear layer (ONL) and synaptic terminals of the photoreceptor cells in wt mouse retina. Immunoreactivity was also detected in other portions of the retina, including the outer plexiform layer (OPL), around cell bodies in the inner nuclear layer (INL), the inner plexiform layer (IPL) and ganglion cell layer (GCL) (Fig. 3A). High magnification shows that staining was present throughout the OPL, indicating that dynamin-1 is localized to the photoreceptor terminals as well as the postsynaptic dendrites of the second-order neurons.

Since an association exists between Tulp1 and dynamin-1 (Xi *et al.*, 2007), we examined dynamin-1's localization in the *tulp1*−/− retina (Fig. 3B). Figure 3B indicates that the localization of dynamin-1 in the *tulp1*−/− retina appears similar to that in the wt retina with immunoreactivity seen in the IS, ONL, OPL, INL, IPL and GCL. These results imply that the absence of Tulp1 does not grossly affect the retinal distribution of dynamin-1.

In contrast to the broad staining pattern of dynamin-1 in the wt retina, dynamin-2 immunoreactivity was found predominantly above the myoid region of the IS (Fig. 3C). The myoid region is the proximal portion of the IS which houses the machinery for protein translation including the Golgi apparatus and endoplasmic reticulum. High magnification indicates that dynamin-2 localizes near the region of the connecting cilium (CC), the intracellular link between the functionally different compartments of the IS and OS (Fig. 3C). This is in agreement with proteomic data from CC preparations (Liu *et al.*, 2007). There was also dynamin-2 staining in the OPL, IPL and GCL, but much less pronounced as compared to dynamin-1. Dynamin-3 localization in the wt retina was most apparent in the

NIH-PA Author Manuscript

NIH-PA Author Manuscript

NIH-PA Author Manuscript

IPL (Fig. 3D). Immunoreactivity was also detected in the IS, OPL, INL and GCL. Finally, a pan-dynamin antibody appears to label much of the neural retina, similar to dynamin-1 (Fig. 3E). The localization patterns of dynamin isoforms in wt and *tulp1−/−* mice were similar at earlier (P13) and later ages (P21) (data not shown).

Dynamin-1 interacting proteins in the mouse retina

To identify dynamin-1 interacting proteins, we performed IPs from wt mouse retinal homogenates using a dynamin-1 specific antibody. Two independent IP experiments were performed and figure 4 shows a representative SDS-PAGE result. The IP and control lanes were excised into 31 fractions and proteins in each were identified by LC MS/MS. The major Coomassie blue band at ~100 kDa (Fig. 4A) was identified in both independent experiments as dynamin-1 (based on 83% sequence coverage). In addition, western blot analysis with anti-dynamin-1 also identified the 100 kDa band as dynamin-1 (Fig. 4B). Subsequent western blot analysis with anti-Tulp1 supported Tulp1 as a constituent of a dynamin-1 protein complex in the wt mouse retina but not in the *tulp1−/−* retinal lysate (Fig. 4C). In a separate experiment, Tulp1 was also detected by western blot analysis of dynamin-1 IP products from bovine retinal homogenates (data not shown). Tulp1 was not identified in an IP from wt retina using non-specific IgG antibodies or in an IP from *tulp1−/−* retina using dynamin-1 antibodies (Fig. 4D).

Proteomic analyses of the anti-dynamin-1 IP products from mouse retina identified 128 proteins (Supplementary Table 1). Table 2 presents a summary of the 50 proteins identified in two IP experiments that were not identified in control IP experiments using non-specific IgG. These 50 proteins were classified into nine functional groups using bioinformatic methods, with several proteins categorized into more than one group (Fig. 5). The three most prevalent functional categories were cytoskeletal-associated, membrane dynamics and transport, and synaptic processes (Fig. 5). Sixteen proteins were classified as members of the cytoskeleton, fourteen were involved in membrane dynamics and vesicular protein transport and nine were synaptic proteins. Other categories containing fewer proteins included mRNA processing, cell adhesion, ion transport, translation and mitochondrial-associated.

To determine whether these potential dynamin-1 interactions are retina-specific or ubiquitous, we conducted parallel IPs in wt mouse brain tissue. Two independent brain IP experiments were performed and non-specific IgG was used as a control. As performed in retinal experiments, the IP and control lanes were excised into 31 fractions and proteins in each were identified by LC MS/MS. Proteomic analyses of the anti-dynamin-1 IP products from mouse brain identified 132 proteins (Supplementary Table 2). Nineteen proteins were identified in two IP experiments that were not identified in control IP experiments using non-specific IgG (Supplementary Table 3). Of these, seven proteins were identical between retina and brain. These include actin-alpha 2, cadherin 2, catenin alpha-2, catenin beta-1, dynamin-1, dynamin-3 and SRC kinase signaling inhibitor 1. All seven proteins can be classified into the functional categories of cytoskeletal-associated or membrane dynamics and transport.

We further validated seven identified protein partners of dynamin-1 in the retina: clathrin, dynamin-3, lima1, myosin 10, rhodopsin and spectrin by western blot analysis of IP complexes (Fig. 6). These are representative proteins of the three major functional classes of dynamin-1 interacting partners – cytoskeletal, membrane dynamics and transport and synaptic. All seven proteins were clearly detected in the retinal IP samples but not in the control IP samples, indicating that these proteins interact with dynamin-1. The abundant brain protein, myelin basic protein (MBP), was used as a brain-specific control; peripherin was used as retina-specific control. In agreement with our proteomic data, peripherin and

NIH-PA Author Manuscript

NIH-PA Author Manuscript

NIH-PA Author Manuscript

MBP were not detected in the IP product lanes of their respective tissues; however, they were present in the appropriate lysate preparations (Fig. 6).

Discussion

Dynamins play important roles in neurons of the central nervous system, where they generate vesicles from membranes (Ferguson & De Camilli, 2012). Herein, we confirm that dynamins -1, -2, and -3 are expressed in the retina and are present in multiple classes of retinal neurons. Furthermore, our results indicate that each isoform has a distinct pattern of distribution throughout the retina.

The broad cellular localization of dynamin-1 is similar to that seen using a pan-dynamin antibody (Fig. 3A and E), indicating that dynamin-1 is the dominant isoform in the mouse retina, as has been postulated for the mouse brain (Ferguson *et al.*, 2007). In contrast to dynamin-1, dynamin-2 localization is highly concentrated above the myoid region of the IS near the CC (Fig. 3C). The CC represents a transition zone between the IS and OS and plays a key role in the transport of proteins as they are synthesized in the IS and trafficked to the OS (Insinna & Besharse, 2008). This suggests that dynamin-2 plays a role in intracellular transport in the photoreceptor cell, as has been proposed for other cell types (Cao *et al.*, 1998). Dynamin-3 expression is most pronounced in the IPL where synaptic terminals of second order bipolar neurons synapse with amacrine and ganglion cells (Fig. 3D). Dynamin-3 is also present throughout the OPL, and appears to be expressed in photoreceptor terminals and the dendrites of second order neurons. These results suggest that dynamin-3 plays a critical role in retinal synaptic processing.

Dynamin-1 and Tulp1 interact in photoreceptor cells and co-localize in the IS, ONL and OPL (Xi *et al.*, 2007). Although Tulp1 was below detection limits by mass spectroscopy in mouse retina, we confirm the interaction of these two proteins by western blot analysis in both mouse and bovine retinas (Fig. 4). Tulp1 is a photoreceptor–specific protein which associates with the cytoskeleton and plays a role in intracellular protein transport (Hagstrom *et al.*, 1999; Xi *et al.*, 2005; Xi *et al.*, 2007; Grossman *et al.*, 2009). *Tulp1*−/− mice develop early-onset photoreceptor degeneration with defects in protein vesicular transport (Hagstrom *et al.*, 1999; Hagstrom *et al.*, 2001; Grossman *et al.*, 2009; Grossman *et al.*, 2011). Several proteins are not transported correctly to the OS in *tulp1*−/− retinas (Grossman *et al.*, 2011); therefore, we investigated whether dynamin-1 localization was influenced in the absence of Tulp1. Surprisingly, dynamin-1 expression and localization did not appear to be affected in *tulp1*−/− retinas (Figs. 2 and 3). In fact, all three dynamin isoform protein levels were comparable in wt and *tulp1*−/− retinas, thus excluding dynamin-1 mislocalization as part of the retinal degenerative process observed in *tulp1*−/− mice.

Fifty proteins were identified in two retinal anti-dynamin-1 IPs, suggesting that these proteins may interact with dynamin-1 in mouse retina *in vivo* (Table 2). Of these, 30 were either constituents of the cytoskeleton or involved in membrane dynamics and transport (Fig. 5). This is not surprising given that there is a bi-directional interaction between cytoskeleton proteins and cellular membranes (Doherty & McMahon, 2008). Furthermore, the dynamin proteins have been shown to function in vesicle movement in association with cytoskeleton elements in neurons of the central nervous system (Ferguson *et al.*, 2007; Jaiswal *et al.*, 2009). Our protein interaction results suggest that a similar model applies to retinal neurons. Although there are differences between the dynamin-1 protein constituents between retina and brain, the majority of the proteins identified in both retina and brain are involved in either membrane dynamics and transport or associated with the cytoskeleton (Supplementary Tables 2 and 3). The cytoskeleton is the cellular scaffolding composed of microfilaments, intermediate filaments and microtubules that is critical in membrane

NIH-PA Author Manuscript

NIH-PA Author Manuscript

NIH-PA Author Manuscript

dynamics such as endocytosis at the synapse (Mooren *et al.*, 2012), vesicle generation at the trans-Golgi face (Stow & Heimann, 1998) and motor-driven intracellular vesicular protein transport (Anitei & Hoflack, 2012). We identified several potential retinal dynamin-1 interacting proteins that comprise the filamentous scaffolding of the cytoskeleton including actin, tubulin, neurofilament polypeptide, rootletin and lima1, as well as proteins which modulate or stabilize these networks, such as nestin, spectrin, MAP1B and catenin. Several of these proteins were validated by western blot analysis indicating that these proteins likely interact with dynamin-1 *in vivo* (Fig. 6)

A graphic depiction of the highly polarized and compartmentalized photoreceptor cell is shown in Figure 7. The three regions where dynamin-1 and Tulp1 co-localize (Fig. 7, shaded in orange) exhibit high levels of cytoskeleton-dependent vesicular transport and extensive membrane dynamics. The compartment-specific biological processes include OS protein transport (Fig. 7A), axonal transport (Fig. 7B), and synaptic vesicle transport and membrane retrieval (Fig. 7C).

Photoreceptor OS-specific proteins are packaged into vesicles generated at the trans-Golgi face and transported through the CC (Fig. 7A). All three dynamin isoforms have been shown to function in vesicle generation at the trans-Golgi face (Cao *et al.*, 1998). In support of this role, we identified members of the spectrin protein family as dynamin-1 binding partners. Spectrins associate with the cytoskeleton and play a role in protein transport from the trans-Golgi network (Fath *et al.*, 1997). In mammalian photoreceptors, there appears to be several distinct post-Golgi vesicle transport pathways (Grossman *et al.*, 2011), some of which are linked to myosin-based movement (Liu *et al.*, 1999). The myosin family is composed of actin-based motor proteins that are responsible for many diverse functions including intracellular transport (Syamaladevi *et al.*, 2012). We identified several members of the myosin family as potential dynamin-1 retinal binding partners, including myosin VI. Myosin VI is localized to the IS region and has been implicated in cargo sorting and vesicle formation at the trans-Golgi face (Warner *et al.*, 2003; Kitamoto *et al.*, 2005). Important to both vesicle generation and transport in the IS, the non-muscle cell α and γ actin isoforms were identified in our IP analyses. Actin microfilaments perform many cellular functions not the least of which is to provide tracks for the myosins to transport cargo. In addition to the actin-based transport pathways, there are distinct microtubule networks in the IS and CC of the photoreceptor which are critical in the transport of OS proteins (Whitehead *et al.*, 1999). Previous studies suggest that the dynamins stabilize microtubule networks (Tanabe & Takei, 2009). We identified α-tubulin, a component of microtubules, as a possible dynamin-1 binding partner.

A second region where there is vesicular transport in the photoreceptor cell is throughout the axon (Fig. 7B). Protein transport in the axon is bi-directional and relies on microtubule-based motor proteins (Schwartz, 1979). Here too, the dynamins may regulate the stability of axonal microtubule networks (Tanabe & Takei, 2009). Pertinent to this role, we identified microtubule-associated protein 1B (MAP1B) as a potential dynamin-1 interacting protein. MAP1B is expressed primarily in neurons where it functions in stabilizing microtubules (Halpain & Dehmelt, 2006). We have localized MAP1B to the ONL (Grossman *et al.*, 2012a), where it may interact with Tulp1 (Xi *et al.*, 2003). Interestingly, Tulp1 exhibits a genetic interaction with a gene for the related protein, MAP1A, whereby an allele of the gene significantly attenuates photoreceptor degeneration in Tulp1 mutant mice (Maddox *et al.*, 2012). Both MAP1A and Tulp1 have been shown to bind tubulin and actin, linking the microtubule networks to the microfilament cytoskeleton (Noiges *et al.*, 2002; Xi *et al.*, 2003; Xi *et al.*, 2005). These results indicate that interactions between dynamin-1, MAPs and Tulp1 may contribute to the stability of these networks and modulate protein movement along these networks.

NIH-PA Author Manuscript

NIH-PA Author Manuscript

NIH-PA Author Manuscript

The synaptic terminal is also reliant upon continuous membrane remodeling and vesicle cycling (Fig. 7C). Synaptic membrane events are highly coordinated by the cytoskeleton to replenish synaptic vesicles and compensate for increases in membrane area due to exocytosis. Synaptic proteins were the third largest category of potential dynamin-1 interacting proteins in our study, and included proteins exclusive to synaptic vesicle transport and membrane retrieval such as src kinase signaling inhibitor 1 and V-type proton ATPase 116 kDa subunit a isoform 1.

The dynamins have long been associated with clathrin-mediated endocytosis (CME) and clathrin-independent endocytosis (van der Bliek & Meyerowitz, 1991). The dynamin-1 (a,c) retinal splice-variant has a frameshift mutation which terminates the protein at amino acid 814 (Xi *et al.*, 2007), eliminating the last 53 amino acids in the proline-rich domain (PRD). Many proteins of the CME pathway bind to the PRD of dynamin, including the amphiphysins, endophilins and syndapins (Anggono & Robinson, 2007). In agreement with this model, none of these proteins were detected in this study. However, rho GTPase-activating protein 32 was identified, which has been shown to regulate clathrin-independent endocytic pathways (Qualmann & Mellor, 2003; Lundmark *et al.*, 2008).

Although our study focused primarily on dynamin-1, dynamin-3 may also perform important functions in the retina. Dynamin-3 staining was strongest in the IPL, but immunoreactivity was also seen in the IS and at the photoreceptor terminal (Fig. 3D). Self-assembly of dynamin polymers has been shown to involve the GTPase, middle and GED domains (Smirnova *et al.*, 1999), all of which are present in the retina-specific dynamin-1 splice-variant (Xi *et al.*, 2007). Therefore, we hypothesize that this dynamin-1 isoform maintains this essential ability. In our study, dynamin-3 was identified and confirmed as a dynamin-1 binding partner, suggesting that different isoforms may have *in vivo* interactions in the retina. Indeed, there is recent evidence that dynamin-1 and -3 isoforms cooperate in promoting activity-dependent synaptic vesicle endocytosis in neurons of the brain (Raimondi *et al.*, 2011).

Twenty other apparent dynamin-1 interacting proteins fell into additional categories. Several are important to mitochondrial function. Although not previously attributed to dynamin-1, members of the dynamin superfamily are known to be involved in mitochondrial fission and fusion (Ferguson & De Camilli, 2012). Proteins involved in cell adhesion were also identified. This is not surprising, given that there is an association between the cytoskeleton and cell adhesion matrices (Kaibuchi *et al.*, 1999). Finally, although the dynamins are not known to function in translation or transcription, we identified several proteins in these groups, perhaps indicating expanded retinal roles for this isoform.

In conclusion, all three dynamin isoforms are expressed in the mouse retina with distinct localization patterns. Dynamin-1 exhibits the broadest localization and appears to be the primary isoform in the retina. Dynamin-1 localizes to specialized compartments of the photoreceptor and many of the potential interacting proteins can be grouped into cytoskeleton and membrane modeling categories, participating in intracellular transport processes relevant to endocytic and post-Golgi pathways. In addition, dynamin-1 may be important for photoreceptor cellular stability. Nevertheless, several of these proteins are specific to distinct pathways, suggesting that dynamin-1 may have compartment-specific interactomes. This has recently been proposed for Tulp1 (Grossman *et al.*, 2012b). Additional analyses are necessary to support this idea and to expand upon the role of dynamins in the retina, including differentiating cell-type-specific functions and splice-variant contributions.

NIH-PA Author Manuscript

NIH-PA Author Manuscript

NIH-PA Author Manuscript

Supplementary Material

Refer to Web version on PubMed Central for supplementary material.

References

Adamus G, Zam ZS, Arendt A, Palczewski K, McDowell JH, Hargrave PA. Anti-rhodopsin monoclonal antibodies of defined specificity: characterization and application. Vision Res. 1991; 31:17–31. [PubMed: 2006550]

Anggono V, Robinson PJ. Syndapin I and endophilin I bind overlapping proline-rich regions of dynamin I: role in synaptic vesicle endocytosis. J Neurochem. 2007; 102:931–943. [PubMed: 17437541]

Anitei M, Hoflack B. Bridging membrane and cytoskeleton dynamics in the secretory and endocytic pathways. Nat Cell Biol. 2012; 14:11–19. [PubMed: 22193159]

Cao H, Garcia F, McNiven MA. Differential distribution of dynamin isoforms in mammalian cells. Mol Biol Cell. 1998; 9:2595–2609. [PubMed: 9725914]

Crabb JW, Miyagi M, Gu X, Shadrach K, West KA, Sakaguchi H, Kamei M, Hasan A, Yan L, Rayborn ME, Salomon RG, Hollyfield JG. Drusen proteome analysis: an approach to the etiology of age-related macular degeneration. Proc Natl Acad Sci U S A. 2002; 99:14682–14687. [PubMed: 12391305]

Daley WP, Gulfo KM, Sequeira SJ, Larsen M. Identification of a mechanochemical checkpoint and negative feedback loop regulating branching morphogenesis. Dev Biol. 2009; 336:169–182. [PubMed: 19804774]

Doherty GJ, McMahon HT. Mediation, modulation, and consequences of membrane-cytoskeleton interactions. Annu Rev Biophys. 2008; 37:65–95. [PubMed: 18573073]

Fath KR, Trimbur GM, Burgess DR. Molecular motors and a spectrin matrix associate with Golgi membranes in vitro. J Cell Biol. 1997; 139:1169–1181. [PubMed: 9382864]

Ferguson SM, Brasnjo G, Hayashi M, Wolfel M, Collesi C, Giovedi S, Raimondi A, Gong LW, Ariel P, Paradise S, O'Toole E, Flavell R, Cremona O, Miesenbock G, Ryan TA, De Camilli P. A selective activity-dependent requirement for dynamin 1 in synaptic vesicle endocytosis. Science. 2007; 316:570–574. [PubMed: 17463283]

Ferguson SM, De Camilli P. Dynamin, a membrane-remodelling GTPase. Nat Rev Mol Cell Biol. 2012

Gray NW, Fourgeaud L, Huang B, Chen J, Cao H, Oswald BJ, Hemar A, McNiven MA. Dynamin 3 is a component of the postsynapse, where it interacts with mGluR5 and Homer. Curr Biol. 2003; 13:510–515. [PubMed: 12646135]

Grossman, GH.; Beight, C.; Ebke, LE.; Hagstrom, SA. Interaction of Tulp1 and the Microtubule-associated Proteins in the Murine Retina. 2012a.

Grossman GH, Pauer GJ, Hoppe G, Hagstrom SA. Isolating photoreceptor compartment-specific protein complexes for subsequent proteomic analysis. Adv Exp Med Biol. 2012b; 723:701–707. [PubMed: 22183396]

Grossman GH, Pauer GJ, Narendra U, Peachey NS, Hagstrom SA. Early synaptic defects in tulp1−/− mice. Invest Ophthalmol Vis Sci. 2009; 50:3074–3083. [PubMed: 19218615]

Grossman GH, Watson RF, Pauer GJ, Bollinger K, Hagstrom SA. Immunocytochemical evidence of Tulp1-dependent outer segment protein transport pathways in photoreceptor cells. Exp Eye Res. 2011; 93:658–668. [PubMed: 21867699]

Hagstrom SA, Adamian M, Scimeca M, Pawlyk BS, Yue G, Li T. A role for the Tubby-like protein 1 in rhodopsin transport. Invest Ophthalmol Vis Sci. 2001; 42:1955–1962. [PubMed: 11481257]

Hagstrom SA, Duyao M, North MA, Li T. Retinal degeneration in tulp1−/− mice: vesicular accumulation in the interphotoreceptor matrix. Invest Ophthalmol Vis Sci. 1999; 40:2795–2802. [PubMed: 10549638]

Hagstrom SA, North MA, Nishina PL, Berson EL, Dryja TP. Recessive mutations in the gene encoding the tubby-like protein TULP1 in patients with retinitis pigmentosa. Nat Genet. 1998; 18:174–176. [PubMed: 9462750]

NIH-PA Author Manuscript

NIH-PA Author Manuscript

NIH-PA Author Manuscript

Halpain S, Dehmelt L. The MAP1 family of microtubule-associated proteins. Genome Biol. 2006; 7:224. [PubMed: 16938900]

Han MY, Kosako H, Watanabe T, Hattori S. Extracellular signal-regulated kinase/mitogen-activated protein kinase regulates actin organization and cell motility by phosphorylating the actin cross-linking protein EPLIN. Mol Cell Biol. 2007; 27:8190–8204. [PubMed: 17875928]

Holroyd P, Lang T, Wenzel D, De Camilli P, Jahn R. Imaging direct, dynamin-dependent recapture of fusing secretory granules on plasma membrane lawns from PC12 cells. Proc Natl Acad Sci U S A. 2002; 99:16806–16811. [PubMed: 12486251]

Insinna C, Besharse JC. Intraflagellar transport and the sensory outer segment of vertebrate photoreceptors. Dev Dyn. 2008; 237:1982–1992. [PubMed: 18489002]

Jaiswal JK, Rivera VM, Simon SM. Exocytosis of post-Golgi vesicles is regulated by components of the endocytic machinery. Cell. 2009; 137:1308–1319. [PubMed: 19563761]

Jeub M, Bitoun M, Guicheney P, Kappes-Horn K, Strach K, Druschky KF, Weis J, Fischer D. Dynamin 2-related centronuclear myopathy: clinical, histological and genetic aspects of further patients and review of the literature. Clin Neuropathol. 2008; 27:430–438. [PubMed: 19130742]

Kaibuchi K, Kuroda S, Amano M. Regulation of the cytoskeleton and cell adhesion by the Rho family GTPases in mammalian cells. Annu Rev Biochem. 1999; 68:459–486. [PubMed: 10872457]

Kelly BL, Vassar R, Ferreira A. Beta-amyloid-induced dynamin 1 depletion in hippocampal neurons. A potential mechanism for early cognitive decline in Alzheimer disease. J Biol Chem. 2005; 280:31746–31753. [PubMed: 16002400]

Kinuta M, Yamada H, Abe T, Watanabe M, Li SA, Kamitani A, Yasuda T, Matsukawa T, Kumon H, Takei K. Phosphatidylinositol 4,5-bisphosphate stimulates vesicle formation from liposomes by brain cytosol. Proc Natl Acad Sci U S A. 2002; 99:2842–2847. [PubMed: 11867768]

Kitamoto J, Libby RT, Gibbs D, Steel KP, Williams DS. Myosin VI is required for normal retinal function. Exp Eye Res. 2005; 81:116–120. [PubMed: 15978262]

Linton JD, Holzhausen LC, Babai N, Song H, Miyagishima KJ, Stearns GW, Lindsay K, Wei J, Chertov AO, Peters TA, Caffe R, Pluk H, Seeliger MW, Tanimoto N, Fong K, Bolton L, Kuok DL, Sweet IR, Bartoletti TM, Radu RA, Travis GH, Zagotta WN, Townes-Anderson E, Parker E, Van der Zee CE, Sampath AP, Sokolov M, Thoreson WB, Hurley JB. Flow of energy in the outer retina in darkness and in light. Proc Natl Acad Sci U S A. 2010; 107:8599–8604. [PubMed: 20445106]

Liu Q, Tan G, Levenkova N, Li T, Pugh EN Jr, Rux JJ, Speicher DW, Pierce EA. The proteome of the mouse photoreceptor sensory cilium complex. Mol Cell Proteomics. 2007; 6:1299–1317. [PubMed: 17494944]

Liu X, Udovichenko IP, Brown SD, Steel KP, Williams DS. Myosin VIIa participates in opsin transport through the photoreceptor cilium. J Neurosci. 1999; 19:6267–6274. [PubMed: 10414956]

Lundmark R, Carlsson SR. Sorting nexin 9 participates in clathrin-mediated endocytosis through interactions with the core components. J Biol Chem. 2003; 278:46772–46781. [PubMed: 12952949]

Lundmark R, Doherty GJ, Howes MT, Cortese K, Vallis Y, Parton RG, McMahon HT. The GTPase-activating protein GRAF1 regulates the CLIC/GEEC endocytic pathway. Curr Biol. 2008; 18:1802–1808. [PubMed: 19036340]

Maddox DM, Ikeda S, Ikeda A, Zhang W, Krebs MP, Nishina PM, Naggert JK. An allele of microtubule-associated protein 1A (Mtap1a) reduces photoreceptor degeneration in Tulp1 and Tub mutant mice. Invest Ophthalmol Vis Sci. 2012

McNiven MA, Cao H, Pitts KR, Yoon Y. The dynamin family of mechanoenzymes: pinching in new places. Trends Biochem Sci. 2000; 25:115–120. [PubMed: 10694881]

Mooren OL, Galletta BJ, Cooper JA. Roles for actin assembly in endocytosis. Annu Rev Biochem. 2012; 81:661–686. [PubMed: 22663081]

Nakajima T, Ochi S, Oda C, Ishii M, Ogawa K. Ischemic preconditioning attenuates of ischemia-induced degradation of spectrin and tau: implications for ischemic tolerance. Neurol Sci. 2011; 32:229–239. [PubMed: 20596741]

NIH-PA Author Manuscript

NIH-PA Author Manuscript

NIH-PA Author Manuscript

Noiges R, Eichinger R, Kutschera W, Fischer I, Nemeth Z, Wiche G, Propst F. Microtubule-associated protein 1A (MAP1A) and MAP1B: light chains determine distinct functional properties. J Neurosci. 2002; 22:2106–2114. [PubMed: 11896150]

Qualmann B, Mellor H. Regulation of endocytic traffic by Rho GTPases. Biochem J. 2003; 371:233–241. [PubMed: 12564953]

Raimondi A, Ferguson SM, Lou X, Armbruster M, Paradise S, Giovedi S, Messa M, Kono N, Takasaki J, Cappello V, O'Toole E, Ryan TA, De Camilli P. Overlapping role of dynamin isoforms in synaptic vesicle endocytosis. Neuron. 2011; 70:1100–1114. [PubMed: 21689597]

Rozas JL, Gomez-Sanchez L, Tomas-Zapico C, Lucas JJ, Fernandez-Chacon R. Increased neurotransmitter release at the neuromuscular junction in a mouse model of polyglutamine disease. J Neurosci. 2011; 31:1106–1113. [PubMed: 21248135]

Schwartz JH. Axonal transport: components, mechanisms, and specificity. Annu Rev Neurosci. 1979; 2:467–504. [PubMed: 94249]

Smirnova E, Shurland DL, Newman-Smith ED, Pishvaee B, van der Bliek AM. A model for dynamin self-assembly based on binding between three different protein domains. J Biol Chem. 1999; 274:14942–14947. [PubMed: 10329695]

Stow JL, Heimann K. Vesicle budding on Golgi membranes: regulation by G proteins and myosin motors. Biochim Biophys Acta. 1998; 1404:161–171. [PubMed: 9714787]

Sun TX, Van Hoek A, Huang Y, Bouley R, McLaughlin M, Brown D. Aquaporin-2 localization in clathrin-coated pits: inhibition of endocytosis by dominant-negative dynamin. Am J Physiol Renal Physiol. 2002; 282:F998–1011. [PubMed: 11997316]

Syamaladevi DP, Spudich JA, Sowdhamini R. Structural and functional insights on the Myosin superfamily. Bioinform Biol Insights. 2012; 6:11–21. [PubMed: 22399849]

Tanabe K, Takei K. Dynamic instability of microtubules requires dynamin 2 and is impaired in a Charcot-Marie-Tooth mutant. J Cell Biol. 2009; 185:939–948. [PubMed: 19528294]

Vaid KS, Guttman JA, Babyak N, Deng W, McNiven MA, Mochizuki N, Finlay BB, Vogl AW. The role of dynamin 3 in the testis. J Cell Physiol. 2007; 210:644–654. [PubMed: 17133358]

van der Bliek AM, Meyerowitz EM. Dynamin-like protein encoded by the Drosophila shibire gene associated with vesicular traffic. Nature. 1991; 351:411–414. [PubMed: 1674590]

Warner CL, Stewart A, Luzio JP, Steel KP, Libby RT, Kendrick-Jones J, Buss F. Loss of myosin VI reduces secretion and the size of the Golgi in fibroblasts from Snell's waltzer mice. EMBO J. 2003; 22:569–579. [PubMed: 12554657]

Werner HB, Kuhlmann K, Shen S, Uecker M, Schardt A, Dimova K, Orfaniotou F, Dhaunchak A, Brinkmann BG, Mobius W, Guarente L, Casaccia-Bonnefil P, Jahn O, Nave KA. Proteolipid protein is required for transport of sirtuin 2 into CNS myelin. J Neurosci. 2007; 27:7717–7730. [PubMed: 17634366]

Whitehead JL, Wang SY, Bost-Usinger L, Hoang E, Frazer KA, Burnside B. Photoreceptor localization of the KIF3A and KIF3B subunits of the heterotrimeric microtubule motor kinesin II in vertebrate retina. Exp Eye Res. 1999; 69:491–503. [PubMed: 10548469]

Xi Q, Pauer GJ, Ball SL, Rayborn M, Hollyfield JG, Peachey NS, Crabb JW, Hagstrom SA. Interaction between the photoreceptor-specific tubby-like protein 1 and the neuronal-specific GTPase dynamin-1. Invest Ophthalmol Vis Sci. 2007; 48:2837–2844. [PubMed: 17525220]

Xi Q, Pauer GJ, Marmorstein AD, Crabb JW, Hagstrom SA. Tubby-like protein 1 (TULP1) interacts with F-actin in photoreceptor cells. Invest Ophthalmol Vis Sci. 2005; 46:4754–4761. [PubMed: 16303976]

Xi Q, Pauer GJ, West KA, Crabb JW, Hagstrom SA. Retinal degeneration caused by mutations in TULP1. Adv Exp Med Biol. 2003; 533:303–308. [PubMed: 15180277]

Yang J, Liu X, Yue G, Adamian M, Bulgakov O, Li T. Rootletin, a novel coiled- coil protein, is a structural component of the ciliary rootlet. J Cell Biol. 2002; 159:431–440. [PubMed: 12427867]

Zuchner S, Noureddine M, Kennerson M, Verhoeven K, Claeys K, De Jonghe P, Merory J, Oliveira SA, Speer MC, Stenger JE, Walizada G, Zhu D, Pericak-Vance MA, Nicholson G, Timmerman V, Vance JM. Mutations in the pleckstrin homology domain of dynamin 2 cause dominant intermediate Charcot-Marie-Tooth disease. Nat Genet. 2005; 37:289–294. [PubMed: 15731758]

NIH-PA Author Manuscript

NIH-PA Author Manuscript

NIH-PA Author Manuscript

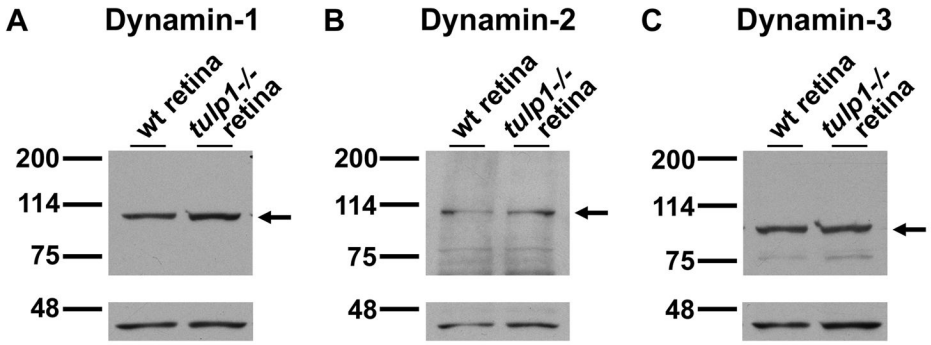

Figure 1.

Multi-tissue analysis indicating that all three dynamin isoforms are present in the P16 mouse retina. (A) Western blot probed with dynamin-1 antibodies. (B) Western blot probed with dynamin-2 antibodies. (C) Western blot probed with dynamin-3 antibodies. Actin is shown in lower blots (~45 kDa) as a control for loading equivalency.

NIH-PA Author Manuscript

NIH-PA Author Manuscript

NIH-PA Author Manuscript

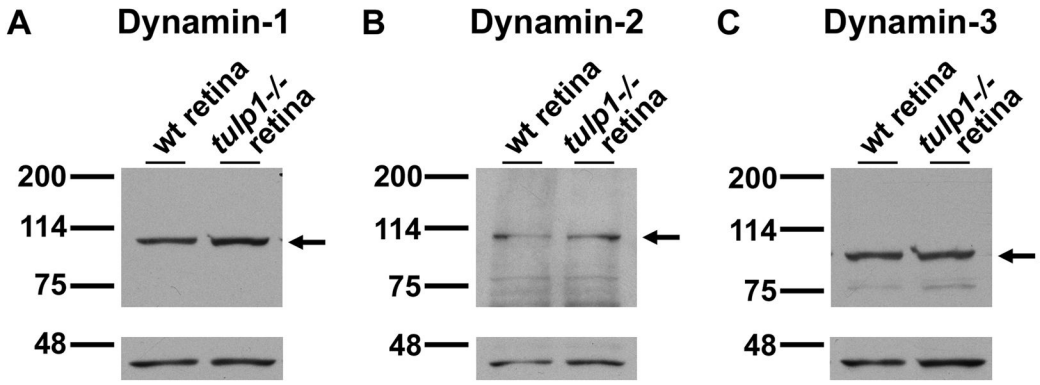

Figure 2.

All three dynamin isoforms are expressed in the P16 wt and *tulp1*−/− mouse retina at similar levels, respectively. (A) Western blot of wt and *tulp1*−/− retinal homogenates probed with dynamin-1 antibodies. In both samples, a single band is present at ~100 kDa at similar levels. (B) Western blot of wt and *tulp1*−/− retinal homogenates probed with dynamin-2 antibodies. In both samples, a major band is present at ~100 kDa at similar levels. (C) Western blot of wt and *tulp1*−/− retinal homogenates probed with dynamin-3 antibodies. In both samples, a single band is present at ~100 kDa at similar levels. Actin is shown in lower blots (~45 kDa) as a control for loading equivalency.

NIH-PA Author Manuscript

NIH-PA Author Manuscript

NIH-PA Author Manuscript

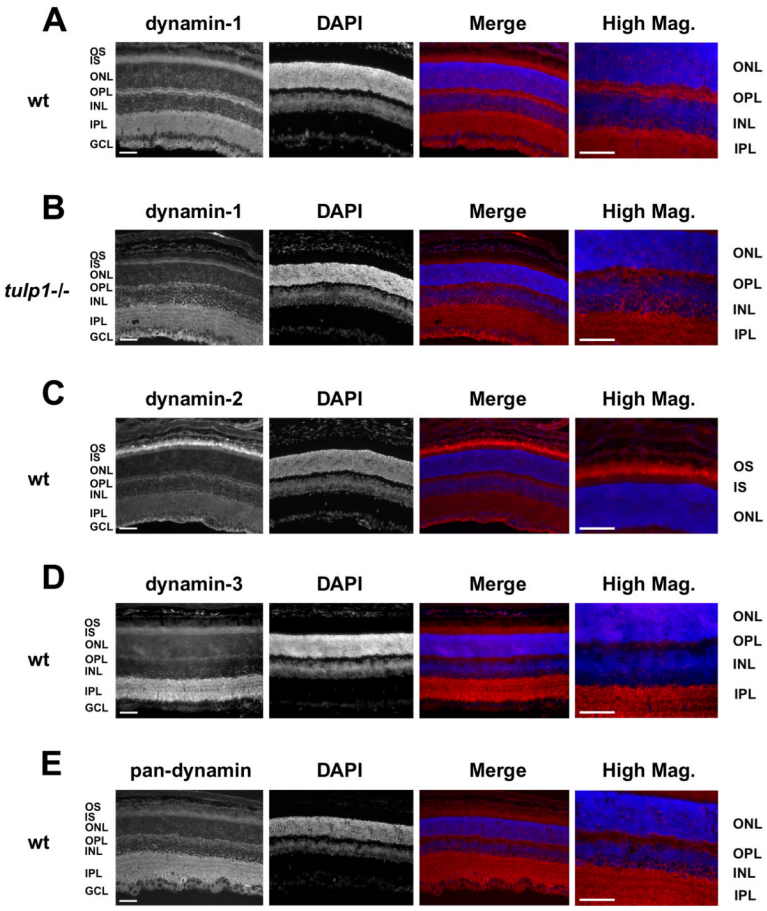

Figure 3.

Immunofluorescent localization of dynamin isoforms in P16 mouse retinal sections. Images of dynamin proteins (first column and pseudo-colored red in the merged images) and nuclei labeled with DAPI (second column and pseudo-colored blue in the merged images) compare the localization of dynamin isoforms. (A) In the wt retina, dynamin-1 staining is present in the IS, ONL, OPL, INL, IPL and GCL. In the fourth column, showing a magnified view, staining is present throughout the OPL, indicating that dynamin-1 is localized to the photoreceptor terminals as well as the postsynaptic dendrites of the second-order neurons. (B) In the *tulp1*−/− retina, dynamin-1 staining exhibits the same pattern as in the wt, signifying that dynamin-1 localization is unaffected in the absence of tulp1. (C) Dynamin-2 immunoreactivity is detected in the IS, OPL, IPL and GCL; however, the magnified view shows that the signal is most concentrated above the myoid region of the IS. (D) Dynamin-3 expression is predominantly localized to the IPL. Less signal is detected in the IS, OPL, INL and GCL. (E) A pan-dynamin antibody that was raised against an epitope shared by all three isoforms shows a staining pattern similar to that of dynamin-1, with immunoreactivity in the IS, ONL, OPL, INL, IPL and GCL. Scale bars = 50 μm.

NIH-PA Author Manuscript
NIH-PA Author Manuscript
NIH-PA Author Manuscript

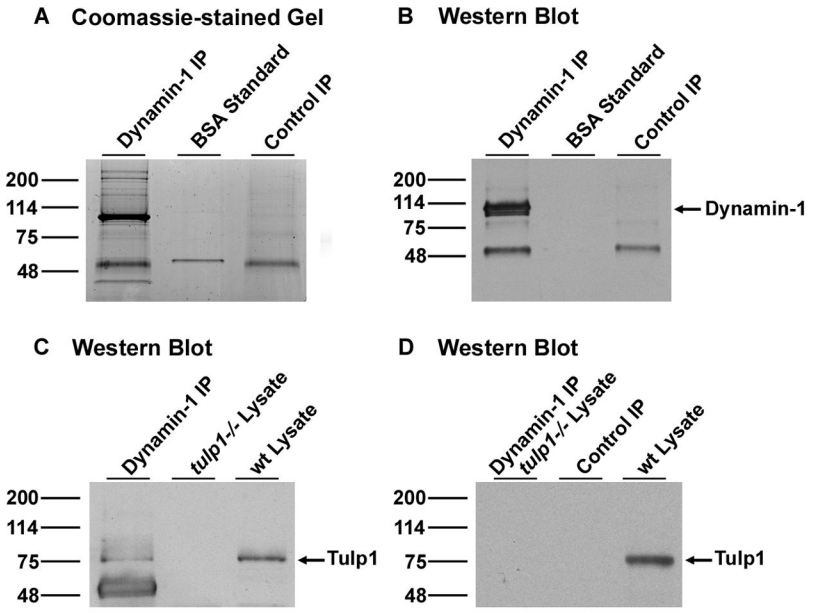

Figure 4.

Immunoprecipitation of a dynamin-1 complex from the mouse retina. (A) Gel Code Blue stain of an SDS-PAGE gel separating retinal lysates incubated with dynamin-1 antibodies. Lane 1: Proteins immunoprecipitated with dynamin-1 antibodies. Lane 2: BSA standard. Lane 3: Proteins immunoprecipitated with rabbit IgG antibodies, serving as a negative control. Lanes 1 and 3 were excised into 2mm segments, digested with trypsin, and the peptides identified by LC MS/MS. (B) Western blot of immunoprecipitation experiment shown in A probed with dynamin-1 antibodies. An arrow points to a major band at ~100 kDa, corresponding to the correct size of the dynamin-1 protein. This band was identified as dynamin-1 by LC MS/MS analysis. The band in lanes 1 and 3 at ~50 kDa was identified as IgG heavy chain. (C) Western blot of a dynamin-1 immunoprecipitation experiment probed with Tulp1 antibodies. Lane 1: Proteins immunoprecipitated with dynamin-1 antibodies. Lane 2: *tulp1−/−* retinal lysate. Lane 3: wt retinal lysate. An arrow points to a major band at ~78 KDa, corresponding to the correct size of the Tulp1 protein, in both the immunoprecipitation product and wt retinal lysate. This band is not seen in the *tulp1−/−* retinal lysate. (D) Western blot of control IP experiments probed with Tulp1 antibodies. Lane 1: Proteins immunoprecipitated with rabbit IgG antibodies from wt retina. Lane 2: Proteins immunoprecipitated with Dynamin-1 antibodies from *tulp1−/−* retina. Lane 3: wt retinal lysate.

NIH-PA Author Manuscript

NIH-PA Author Manuscript

NIH-PA Author Manuscript

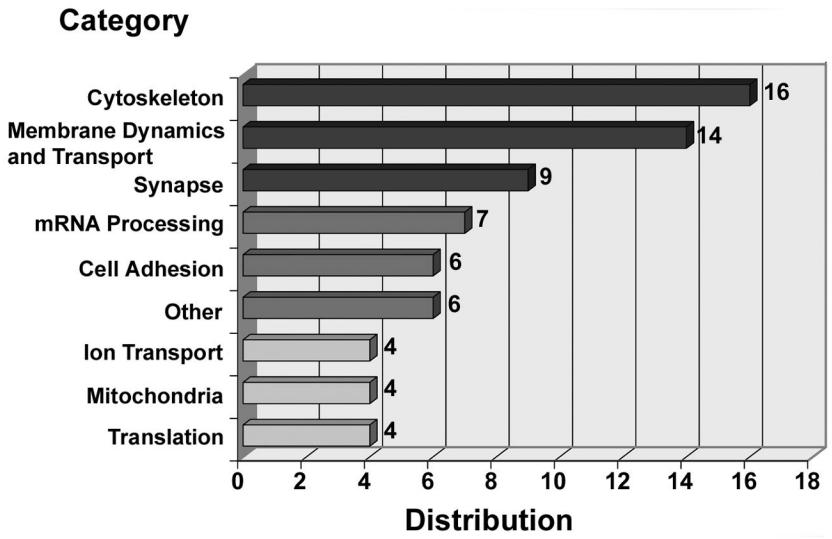

Figure 5.

Bar graph representing the potential dynamin-1 interacting proteins organized by cellular function. Classifications were determined using IPA software and review of protein databases. Each category originates from Table 2 and represents the proteins that were identified in both immunoprecipitation experiments but not in the control experiment. Some proteins are encompassed in more than one functional class. The three most prevalent categories were cytoskeletal, membrane dynamics and transport and synaptic-associated.

NIH-PA Author Manuscript

NIH-PA Author Manuscript

NIH-PA Author Manuscript

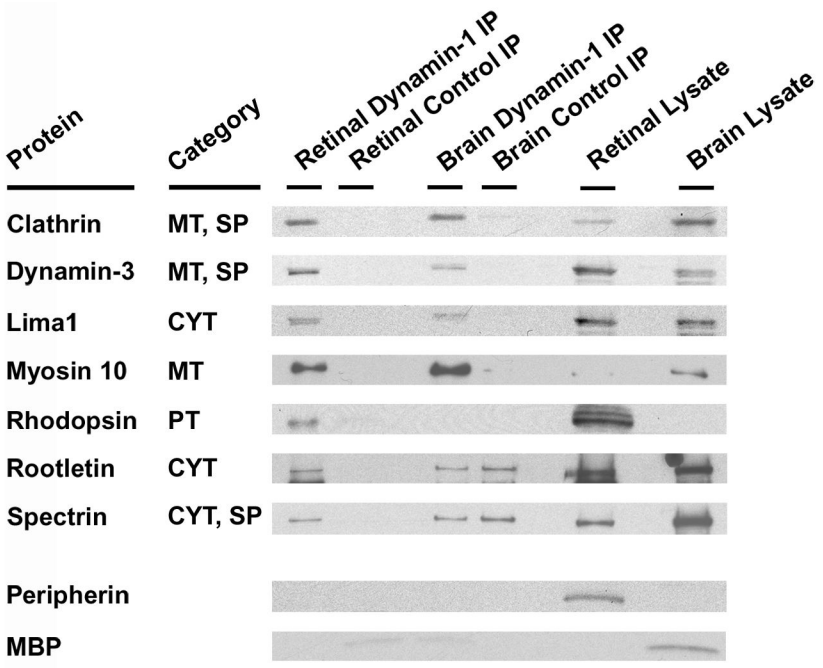

Figure 6.

Western blot analysis validating seven dynamin-1 protein binding partners identified in proteomic analysis. Select proteins from the three most prevalent functional categories are highlighted. The brain and retinal IP complexes were separated by SDS-PAGE and then immunoblotted with the different antibodies as indicated. The category for each protein is indicated. Myelin basic protein (MBP) was used as a brain-specific control; peripherin was used as retina-specific control. CYT: cytoskeleton. MT: membrane dynamics and transport. PT: phototransduction. SP: synapse.

NIH-PA Author Manuscript

NIH-PA Author Manuscript

NIH-PA Author Manuscript

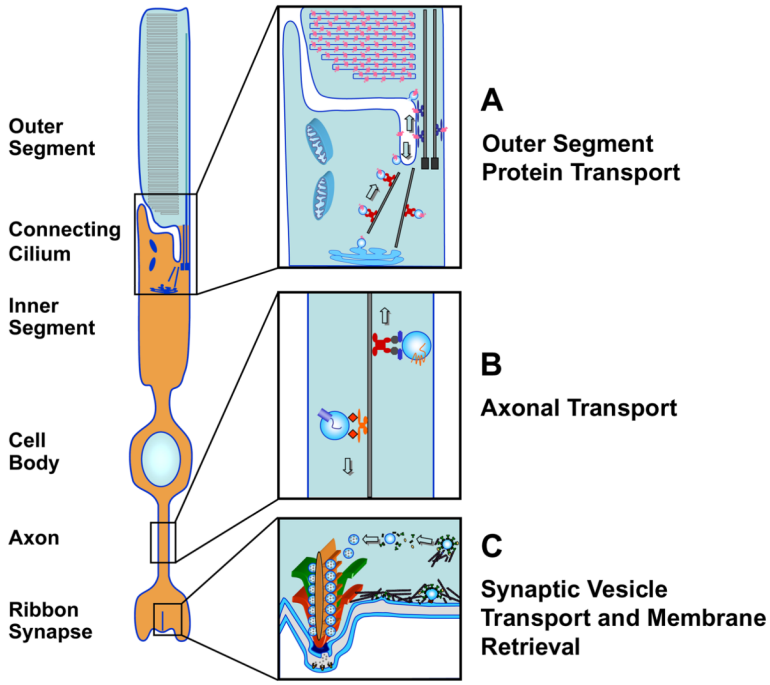

Figure 7.

A graphic depiction of the photoreceptor cell, highlighting the three areas where there are high levels of cytoskeletal-dependent vesicular transport and extensive membrane remodeling. These compartment-specific functions represent the largest categories of dynamin-1 interacting partners, and are active in the regions where dynamin-1 and Tulp1 colocalize (shaded in orange). (A) The inner segment (IS) is the compartment in which outer segment (OS) proteins are processed and packaged into post-Golgi vesicles for transport through the IS and connecting cilium (CC) to the OS disks. (B) Anterograde and retrograde axonal transport allows nascent protein complexes to be trafficked to the photoreceptor synapse and cellular components to be transported back towards the cell body for degradation. (C) At the terminal, endocytosis replenishes synaptic vesicles and compensates for increases in membrane area due to exocytosis.

NIH-PA Author Manuscript NIH-PA Author Manuscript NIH-PA Author Manuscript

NIH-PA Author manuscript; available in PMC 2014 February 27.

Table 1

Primary Antibody Characterization

Protein	Immunogen	Technique/Dilution	Source	Host	Reference
Dynamin-1	Synthetic peptide corresponding to AA residues 633–647 from rat/mouse/human dynamin-1 (EKASETEENGSDSF)	IHC 1:200, WB 1:1,000 and IP 10μg per 500μl retinal lysate	Thermo Scientific, (Rockford, Illinois; PA1-660)	rabbit polyclonal	(Kinuta *et al.*, 2002; Ferguson *et al.*, 2007)
Dynamin-2	Synthetic peptide corresponding to AA residues 760–779 from rat/mouse/human dynamin-2 (SPTPQRRPVSSIHPPGRPPA)	IHC 1:200 and WB 1:1,000	Thermo Scientific, (Rockford, Illinois; PA1-661)	rabbit polyclonal	(Sun *et al.*, 2002; Lundmark & Carlsson, 2003; Kelly *et al.*, 2005)
Dynamin-3	Synthetic C-terminal peptide, specific to dynamin-3 (RLTLSAPLPRPASSRGPAPAIPSPGPHS)	IHC 1:200 and WB 1:1,000	Dr. Mark A. McNiven, (Mayo Clinic, Minneapolis, MN)	rabbit polyclonal	(Cao *et al.*, 1998; Gray *et al.*, 2003; Vaid *et al.*, 2007)
Pan-Dynamin	Synthetic peptide corresponding to AA residues 2–17 of dynamin 1,2 & 3 in rat/ mouse (GNRGMEDLIPLVNRLQ)	IHC 1:100	Synaptic Systems, (Gottingen, Germany; 115 002)	rabbit polyclonal	(Holroyd *et al.*, 2002; Ferguson *et al.*, 2007; Rozas *et al.*, 2011)
Tulp1	Synthetic peptide corresponding to N-terminal AA residues 1–201 of mouse Tulp1	WB 1:1,000	Dr. Stephanie A. Hagstrom, (Mass. Eye and Ear Infirmary, Boston, MA)	rabbit polyclonal	(Hagstrom *et al.*, 2001; Xi *et al.*, 2007; Grossman *et al.*, 2009)
Peripherin	AA residues of the C-terminus of mouse Peripherin (CVEAEGADAGPAPEAG)	IHC 1:500 and WB 1:500	Dr. Andrew F.X. Goldberg, (Oakland Univ., Rochester, MI)	rabbit polyclonal	(Goldberg *et al.*, 2007)
Clathrin	Full length native bovine protein (purified), which recognizes AAs 207–264 of bovine clathrin heavy chains	WB 1:500	Novus Biologicals (Littleton, CO;NB120-11331	mouse monoclonal	(http://www.novusbio.com/Clathrin-heavy-chain-Antibody-TD1_NB120-11331.html)
Lima1	AA residues 700–759 corresponding to human Lima1	WB 1:500	Bethyl Laboratories (Montgomery, TX; 0-103A)	rabbit polyclonal	(Han *et al.*, 2007)
Myelin Basic Protein	Myelin basic protein isolated from human brain	WB 1:200	Dako (Carpinteria, CA; A0623)	rabbit polyclonal	(Werner et al., 2007)
Myosin 10	Synthetic peptide corresponding to the C-terminus of human Myosin 10 (Myosin IIB)	WB 1:500	Cell Signaling Technology (Boston, MA; 3404S)	rabbit polyclonal	(Daley *et al.*, 2009)

NIH-PA Author Manuscript
NIH-PA Author Manuscript
NIH-PA Author Manuscript

Protein	Immunogen	Technique/Dilution	Source	Host	Reference
Rhodopsin	15 AA residues of N-terminal of bovine rhodopsin (MNGTEGPNFYVPFSN)	WB 1:1,000	Dr. Paul Hargrave (University of Florida, Gainesville, FL;R2-15N)	mouse monoclonal	(Adamus et al., 1991)
Spectrin	cell membranes purified by hypotonic lysis and mechanical enucleation	WB 1:400	EMD Millipore (Billerica, MA; MAB1622-Clone AA6)	mouse monoclonal	(Nakajima et al., 2011)
Rootletin	AA residues 1819–2006 of mouse rootletin	WB 1:1000	Dr. Tiansen Li, (National Eye Institute, Bethesda, MD)	rabbit polyclonal	(Yang et al., 2002)

Vis Neurosci. Author manuscript; available in PMC 2014 February 27.

NIH-PA Author Manuscript
NIH-PA Author Manuscript
NIH-PA Author Manuscript

Table 2

Proteins identified in two anti-dynamin-1 immunoprecipitations from mouse retina

	Proteins	Accesion No.	Matches*	Function
1	60 kDa heat shock protein, mitochondrial	P63038	13	MC
2	60S acidic ribosomal protein P0	P14869	5	TL
3	60S ribosomal protein L6	P47911	3	TL
4	60S ribosomal protein L7	P14148	3	TL
5	60S ribosomal protein L18	P35980	2	TL
6	Actin-gamma	P63260	92	CYT
7	Actin-alpha 2	P62737	49	CYT
8	Cadherin-2	P15116	12	CA
9	Cadherin-4	P39038	4	CA
10	Calcium-binding mitochondrial carrier protein Aralar1	Q8BH59	4	MC
11	Catenin alpha-2	Q61301	19	CYT, CA
12	Catenin beta-1	Q02248	15	CA, mRNA, CYT
13	Catenin delta-2	O35927	7	CA, mRNA
14	Clathrin heavy chain 1	Q68FD5	9	MT, SP
15	Cytochrome c oxidase subunit 2	P00405	7	MC
16	Dynamin-1	P39053	306	MT, SP
17	Dynamin-3	Q8BZ98	106	MT, SP
18	Hemoglobin subunit alpha	P01942	8	OX
19	Heterogeneous nuclear ribonucleoprotein M	Q9D0E1	10	mRNA
20	IQ motif and SEC7 domain-containing protein 3	Q3TES0	11	MT, CYT
21	Lima1	Q9ERG0	2	CYT
22	Microtubule-associated protein 1B	P14873	3	CYT, SP, MT
23	Myosin regulatory light chain 12B	Q3THE2	2	MT
24	Myosin-Va	Q99104	23	MT
25	Myosin-VI	Q64331	21	MT
26	Myosin-9	Q8VDD5	17	MT
27	Myosin-10	Q61879	35	MT
28	Myosin-14	Q6URW6	19	MT
29	Nestin	Q6P5H2	2	MT, CYT, NG
30	Neurofilament light polypeptide	P08551	3	CYT, MT
31	6-phosphofructokinase, liver type	P12382	9	GL
32	Plakophilin-4	Q68FH0	9	CA, CYT
33	Protein KIAA1967 homolog	Q8VDP4	6	mRNA
34	RNA-binding protein 14	Q8C2Q3	3	mRNA
35	Rhodopsin	P15409	4	PT
36	Rho GTPase-activating protein 32	Q811P8	8	SP, IS, MT
37	Rootletin	Q8CJ40	7	CYT

NIH-PA Author Manuscript

NIH-PA Author Manuscript

NIH-PA Author Manuscript

	Proteins	Accesion No.	Matches*	Function
38	Serine/arginine-rich splicing factor 1	Q6PDM2	5	mRNA
39	Serine/threonine-protein phosphatase PGAM5, mitochondrial	Q8BX10	6	MC
40	Sodium/potassium-transporting ATPase subunit alpha-2	Q6PIE5	4	IT
41	Spectrin (fodrin) alpha chain, brain	P16546	26	CYT, SP
42	Spectrin (fodrin) beta chain, brain 1	Q62261	25	CYT, SP
43	SRC kinase signaling inhibitor 1	Q9QWI6	29	CYT, SP
44	Testican-2	Q9ER58	2	NG
45	Transcriptional activator protein Pur-beta	O35295	3	mRNA
46	Tropomodulin-2	Q9JKK7	5	CYT
47	Tubulin alpha-4A chain	P68368	14	CYT
48	V-type proton ATPase 116 kDa subunit a isoform 1	Q9Z1G4	12	IT, SP
49	V-type proton ATPase catalytic subunit A	P50516	6	IT
50	V-type proton ATPase subunit d 1	P51863	8	IT

Peptide hits which did not reach statistical significance as determined by Matrix Science Mascot were omitted from the results. All Keratins and Histone H2B types (10 types) were omitted from the results.

*Highest matches within experiments reported

AM: anti-microbial, AP: apoptosis, CA: cell adhesion, CM: cellular metabolism, CJ: cell junction; CP: complement, CYT; cytoskelton,

GL: glycolysis, IS: intracellular signaling, IT: ion transport, MC: Mitochondria, mRNA: mRNA processing,

MT: membrane dynamics and transport, NG: neurogenesis, OX: oxygen binding, PT: phototransduction, SP: synpase, SR: stress response, TL: translation